Desalination and Water Treatment
www.deswater.com
doi: 10.5004/dwt.2021.27137

223 (2021) 403–413
May

TiO_2 subsidized periodic mesoporous organosilicate (TiO_2@PMOS) for facile photodegradation of methyl orange dye

Khurram Shahzad[a], Muhammad Imran Khan[b,*], Shabnam Shahida[c], Abdallah Shanableh[b], Noureddine Elboughdiri[d,e], Shazia Jabeen[f], Suryyia Manzoor[g], Shagufta Zafar[h], Hassan Ali[i], Abdul Waheed Rabbani[j], Javier Fernandez-Garcia[k], Aziz ur Rehman[a,*]

[a]*Department of Chemistry, The Islamia University of Bahawalpur, Bahawalpur 63100, Pakistan, emails: azizypk@yahoo.com (A. ur Rehman), khurramshahzad776@yahoo.com (K. Shahzad)*
[b]*Research Institute of Sciences and Engineering, University of Sharjah, Sharjah 27272, United Arab Emirates, emails: raoimranishaq@gmail.com (M. Imran Khan), shanableh@sharjah.ac.ae (A. Shanableh)*
[c]*Department of Chemistry, University of Poonch, Rawalakot, Azad Kashmir, Pakistan, email: shabnamshahida01@gmail.com*
[d]*Chemical Engineering Department, College of Engineering, University of Ha'il, P.O. Box: 2440, Ha'il 81441, Saudi Arabia, email: ghilaninouri@yahoo.fr*
[e]*Chemical Engineering Process Department, National School of Engineering Gabes, University of Gabes, Gabes 6011, Tunisia*
[f]*Department of Environmental Sciences, The Women University of Multan, Multan 60000, Pakistan, email: shazia.jabeen@iiu.edu.pk*
[g]*Institute of Chemical Sciences, Bahauddin Zakariya University, Multan 60800, Pakistan, email: suryyia.manzoor@bzu.edu.pk*
[h]*Department of Chemistry, The Government Sadiq College Women University, Bahawalpur 63000, Pakistan, email: shg_zf@gscwu.edu.pk*
[i]*Department of Chemistry, Tsinghua University 100084, Beijing, China, email: hassanali471@gmail.com*
[j]*Department of Physics, The Islamia University of Bahawalpur, Bahawalpur 63100, Pakistan, email: Waheed.rabbani@iub.edu.pk*
[k]*Department of Chemical Engineering, University College London, Torrington Place, London, WC1E 7JE, UK, email: j.fernandez.garcia@ucl.ac.uk*

Received 28 September 2020; Accepted 8 February 2021

ABSTRACT

In the present research, we reported TiO_2 subsidized periodic mesoporous organosilicates (TiO_2@PMOS) to reduce organic pollutants by photocatalytic degradation. TiO_2@PMOS was prepared by simply direct adsorbing of TiO_2 onto the PMOS and the PMOS organized on polysorbate 80 ($C_{64}H_{124}O_{26}$) templates through co-condensation of sodium silicate (Na_2SiO_3) and 3-methacryloxypropyltrimethoxysilane ($C_{10}H_{20}O_5Si$). The resultant TiO_2@PMOS were characterized by analytical techniques and showed the successful synthesis of template-assisted PMOS which provided a platform for the preparation of TiO_2@PMOS which exhibited efficient surface area reflected in effective degradation of methyl orange (MO) as an organic azo dye and found 5.36% and 9.02% reduction under visible and UV-lights respectively. Moreover, the addition of H_2O_2 with TiO_2@PMOS produced excessive hydroxyl free radicals which improved the degradation abilities up to 14.55% and 64.63% under visible and under UV-conditions. Results showed that PMOS provided well-support to TiO_2 for photo-degradation of MO due to the availability of long life-time to photo-generated electron–hole pairs. This proficient degradation is recognized to specific incapacitation of metallic nodes into the porous structure of PMOS. Moreover, TiO_2@PMOS were reused several times and showed 53% photocatalytic degradation of MO at optimized conditions. The small decrease in degradation competency of TiO_2@PMOS after several cycles also showed their durability to longtime for the reduction of organic pollutants.

Keywords: Periodic mesoporous silicates; Photocatalytic efficiency; Azo dye; Methylene bridge

* Corresponding authors.

1. Introduction

In the textile industry, cotton, silk, nylon and wool are extensively colored with azo dyes and their excessive amount is released in effluents [1] which becomes harmful and toxic [2], causing environmental problems and forced the researcher for environmental protection [3]. Subsequently, degradation of azo dyes in industrial effluents becomes the need of the hour. Photo-catalysis provided an impressive way to change the previous methods for the treatment of wastewater and disinfection of disease-causing contaminants [4]. Photo-catalysis found to be highly efficient, cost-effective and has a tendency to produce non-toxic and harmless products from pollutants degradation [5]. Modified magnetic ZnO composites also have effective potentials for photo-catalysis and are separable energy tools [6,7]. Periodic mesoporous silicates (PMOS) were a new phase of composites with the hybrid framework of organic and inorganic moieties. These composites were responsible to enhance characteristics on and into the surfaces of catalysts and adsorbents which were quite different from the conventional materials [8]. In the present study, economical TiO_2@PMOS was prepared [9] for photo-degradation of methyl orange (MO) to investigate photocatalytic efficiencies.

Recently, the fabricated nano carbon dots entail graphitic carbon nitride found to be valuable energy carriers [10–12]. Moreover, the mesoporous silica materials acquired massive significance after their discovery [13] and showed electrifying applications after structural modifications in supporting catalysis, adsorption, drug delivery, sensors and chromatography [14]. In the structural-network of PMOS, silicon atoms are in connection with organic moieties such as methyl, ethyl or phenyl and by using multiple precursors of organosilanes all together with definite templates multifunctional PMOS can be synthesized by hydrolysis and condensation reaction. These modifications enhanced the mechanical and optical characteristics of materials and prevent their surfaces from destruction [15]. At present, a large number of PMOS were synthesized for catalytic applications. PMOS modified sulfonic group provided effective reaction sites and consequently used in acid catalysis [16,17]. The surface area and porosity of PMOS facilitated catalytic moieties and metal atoms to combine in the PMOS-framework and also supported charge-transfer characteristics. Likewise, the catalytic modification of PMOS with Au and Ti nanoparticles [18,19] removed the drawbacks such as the heterogeneous distribution of catalytic sites and low stability of the modified surface.

In the present research, initially, PMOS was prepared by using an economical sodium silicate precursor which has many other advantages like low optical loss [20], high thermal resistance [21] and ease in the attachment of organic-inorganic hybrid synthesis [22] and produce more stability [23]. The synthesized PMOS managed direct incorporation of TiO_2 on PMOS surfaces to prepare TiO_2@PMOS rather than using TiO_2 nanoparticles [19]. Finally, photocatalytic efficiencies of TiO_2@PMOS were investigated by facile degradation of methyl orange which proved them an economical and durable catalysis source.

2. Experimental

2.1. Materials

Sodium silicate (Na_2SiO_3), hydrochloric acid (HCl), ethanol (C_2H_5OH), titanium dioxide (TiO_2) and acetone were purchased from Sinopharm Chemical Reagent Co., Ltd., Shanghai, China. 3-methacryloxypropyltrimethoxysilane ($C_{10}H_{20}O_5Si$), lithium aluminum hydride ($LiAlH_4$), methyl orange (MO), hydrogen peroxide (H_2O_2), sodium hydroxide (NaOH), potassium chloride (KCl) and terephthalic acid (TA) were supplied by Sigma Aldrich, Co., Ltd., (Germany). Deionized (DI) water was used throughout this work. All the chemicals were used as received.

2.2. Methods

2.2.1. Synthesis of PMOS

The synthesis of methylene-PMOS was based on the reported methods of hydrolysis and co-condensation with small modification [24–26]. A clear solution of polysorbate 80 templates (0.7 g) and HCl (0.65 g) into 120 g of deionized water was obtained with constant stirring at room temperature. Later on, sodium silicate (1.0 g) with 3-methacryloxypropyltrimethoxysilane (1.70 g) as silicon foundations were added into the mixture and left for 2 h at 45°C with continuous stirring. For aging, the mixture was heated at 85°C for 22 h under constant conditions. The templates were removed from the as-synthesized material using ethanol (380 g) and acetone (280 g) with constant stirring at 56°C for 5 h. The solid product was collected by filtration and washed systematically with deionized water and acetone. The synthesized PMOS was dried in an oven at 100°C for 24 h.

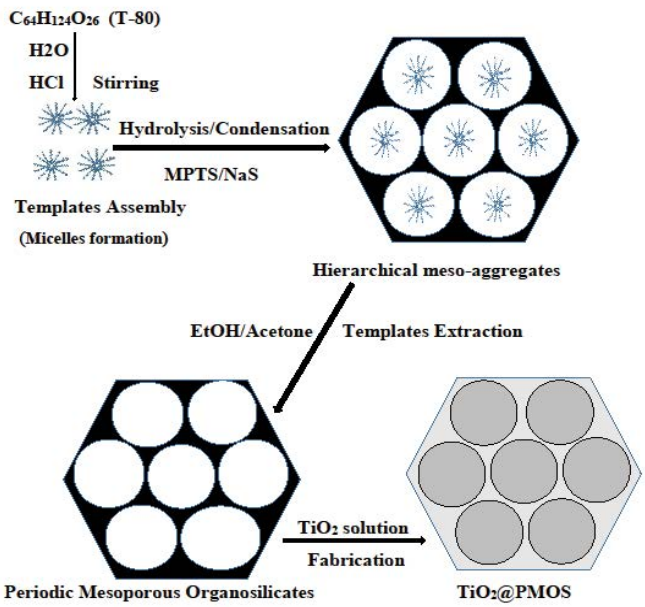

Fig. 1. Schematic design for the template-assisted synthesis of TiO_2@PMOS.

2.2.2. Synthesis of TiO_2@PMOS

Deionized water (80 mL) was used to make a uniform slurry of as-synthesized PMOS (0.7 g) with gentle sonication. Then TiO_2 (0.3 g) was added into the prepared slurry which was almost completely adsorbed onto the PMOS with constant stirring for 5 h. After that $LiAlH_4$ (0.3 g) was mixed to reduce metal-cation if present at room temperature to get TiO_2@PMOS [26] (Fig. 1). The final product was filtered, lightly washed with distilled water and dried in an oven at 100°C for 12 h.

2.3. Characterization

All synthesized PMOS and TiO_2@PMOS were studied by powder X-ray diffraction (XRD) and Fourier-transform infrared spectroscopy (FTIR) for the elucidation of structure. Thermogravimetric analysis (TGA) was used to study the thermal stability of materials. Absorptions were studied by ultraviolet/visible (UV/VIS) spectrophotometry and photoluminescence respectively. Moreover, the surface study was explored by transmission electron microscopy and Brunauer–Emmett–Teller using a nitrogen adsorption instrument.

3. Results and discussion

3.1. Materials synthesis and characterization

Sol–gel synthesis comprised hydrolysis reaction of silicon-precursors in which hydroxyl groups (OH) replaced the alkoxy groups (OR). Organosilica linkages are formed by succeeding co-condensation reactions of silanol groups which consequently formulate PMOS after experienced aging [27]. PMOS provided fine support to TiO_2 for the fabrication and facilitated with a reduction to prepare TiO_2@PMOS. The structure interpretation of PMOS and TiO_2@PMOS was explored by using XRD, FTIR and photoluminescence (PL) analysis techniques.

The progressive structural study of PMOS and TiO_2@PMOS was done by employing XRD pattern. Small nodes were observed in PMOS spectra through wide angle X-ray diffractometer demonstrating the amorphous nature of PMOS [28] which was changed after incorporation of TiO_2 moiety into the orderly crystalline phase (Fig. 2a). XRD pattern of TiO_2@PMOS nanoparticle showed intense diffraction peaks indicating the well-ordered crystalline phase. The most important well resolved peaks indexed as (110), (200), (211), (220) and (221) (Fig. 2a) associated with anatase phase of TiO_2 (JCPDS: 00-002-0406) [29] and supported to the incorporation of organic and TiO_2 moieties in synthesized material [20]. Scherrer's equation, $D = K\lambda/\beta\cos\theta$ was used to calculate crystallite size. Where D represents the average size of crystallite under examination, K and λ have constant values of (0.9) and (1.54056 Å) respectively, β and θ correspond to full-width at half-maximum and diffraction angle of the diffraction peaks [30]. The most intense peaks at 2θ = 34.42 and 40.04 in TiO_2@PMOS spectra were used to determine the average particle size by Scherrer's equation which was found to be 13.41 nm.

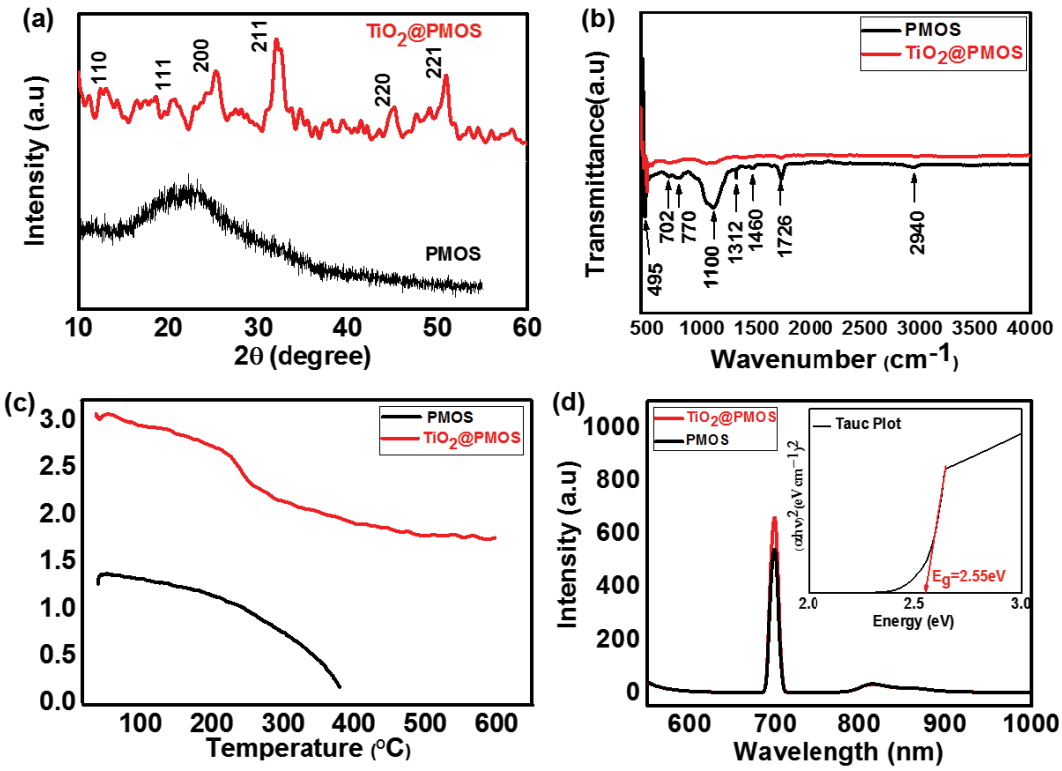

Fig. 2. (a) XRD, (b) FTIR-spectra of PMOS and TiO_2@PMOS, (c) TGA-curves of PMOS and TiO_2@PMOS and (d) PL of PMOS and TiO_2@PMOS with Tauc plot of TiO_2@PMOS.

FTIR analysis substantiated the interactions of PMOS and TiO_2@PMOS (Fig. 2b). The significant peaks at 495; 702; 770; 1,100; 1,312; 1,460; 1,726 and 2,940 per cm indicated that organic and metal moieties successfully integrated into the synthesized materials. The absorption peaks at 702 and 770 cm^{-1} showed the presence of –Si–C and –Si–OCH_3, respectively but significant peaks at 2,940 and 1,460 cm^{-1} exhibited C–H stretching and bending respectively [20,28,31–34]. The stretching vibrations at 1,726 and 1,100 cm^{-1} were due to –C–O–C– and Si–O–Si linkages, respectively [35] revealed mixed bridging of organic and silica moieties in PMOS while a significant peak at 1,312 cm^{-1} was recognition of Si–CH_2 bending [36] indicated the successful anticipation of the organic moiety in synthesized PMOS. The decrease in intensities of PMOS peaks (Fig. 2b) and the characteristic spectral bands at 495 cm^{-1} was due to Ti–O–Ti linkages [29] confirmed the incorporation of TiO_2 moiety into PMOS which made the current research more crucial which also emphasizes the comparatively better efficiency of the direct co-condensation method [37].

TGA was used to study the thermal stability of PMOS and TiO_2@PMOS (Fig. 2c). The operational condition of temperature was 30°C to 1,000°C with a 20°C/min heating rate and 20 mL/min flow-rate of nitrogen gas. PMOS and TiO_2@PMOS samples showed an initial weight loss of 6.9% and 4.74%, respectively due to the loss of water content up to 200°C. Subsequently, the thermogram showed 6.36% weight-loss up to 250°C in TiO_2@PMOS revealed further evaporation of physisorbed solvents but at higher temperatures from 250°C–350°C weight loss was 17.9% and 3.53% in PMOS and TiO_2@PMOS respectively due to the removal of chemisorbed water and organics [28,38]. These results showed that organic moieties present in varying proportions in and onto the material surfaces. Lastly, PMOS and TiO_2@PMOS showed a total mass reduction of 23.6% and 13.29% respectively up to 450°C. Afterward, there was no further destruction occurred in the mesoporous arrangement [28] revealing higher thermal stability of TiO_2@PMOS compared to PMOS.

Photoluminescence (PL) and UV-spectroscopic techniques were used for the optical study of PMOS and TiO_2@PMOS. The synthesized PMOS were found to be active for fluorescence but the same amount of the successful incorporated TiO_2@PMOS showed more intense photoluminescence at a wavelength of 700 nm with bandgap ~2.55 (Fig. 2d) representing the charge transfer point [29].

Transmission electron microscopy (TEM) images (Figs. 3a, b and Figs. S2, S3) exhibited spherical shapes of PMOS-particles and revealed well-ordered particles (Figs. 3c, d and Fig. S4) of TiO_2@PMOS. The magnification of the TEM image (Fig. 3d) indicated the presence of tiny dots of TiO_2 in the network of PMOS. ImageJ software measurements [39] showed an average particle size of 15.42 nm (Fig. S1) favored to an average particle size of TiO_2@PMOS determined by Scherrer's equation.

3.2. Adsorption study

Brunauer–Emmett–Teller (BET) nitrogen adsorption study (Fig. 4 and Figs. S9, S10) showed the highly porous nature of the synthesized PMOS. Likewise, 3.26 nm in pore diameter demonstrated the mesostructure of

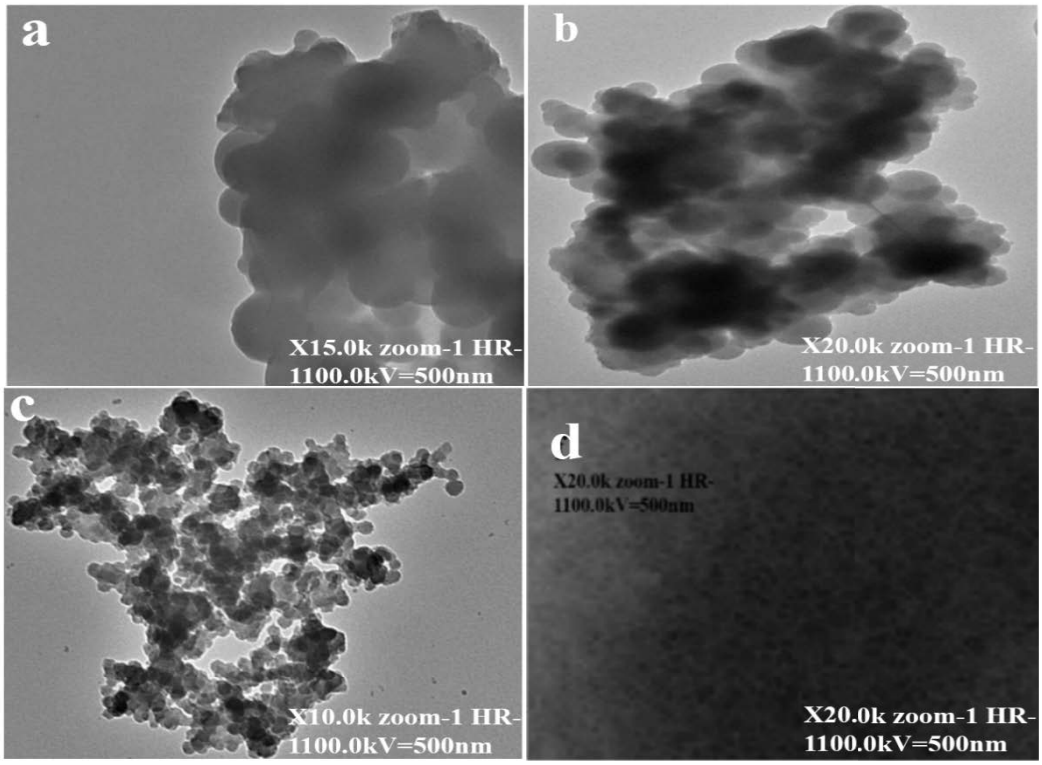

Fig. 3. TEM images of (a and b) PMOS; (c and d) TiO_2@PMOS.

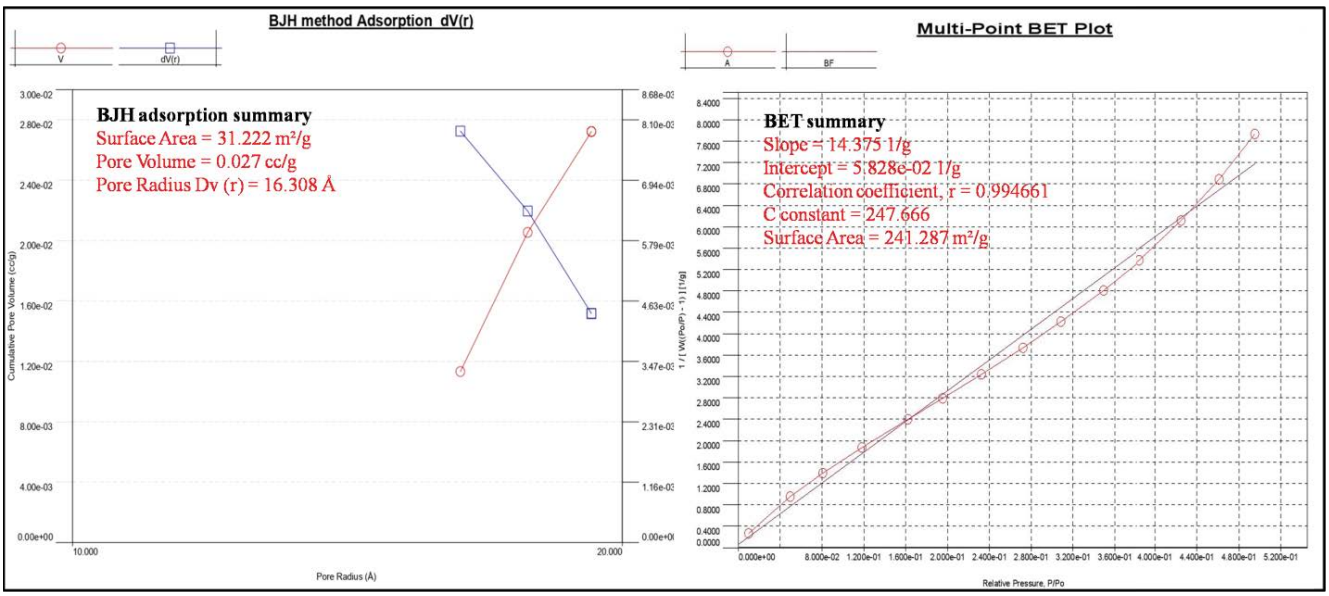

Fig. 4. BET adsorptions study of PMOS.

particles. These proficient properties of PMOS enabled them for high loading of TiO_2 to make TiO_2@PMOS and for catalysis.

3.3. Inspecting •OH generation and degradation mechanism

The generation of hydroxyl free radicals was examined by photoluminescence. In the present study, the hydroxyl free radicals (•OH) were produced by TiO_2@PMOS and chemically changed terephthalic acid (TA) into hydroxylterephthalic acid (TAOH) which was a fluorescent material [40]. The investigation was carried out in a 4 mL aqueous solution of 0.01 M NaOH accompanying 3 mM of TA, 0.03 mM of H_2O_2 (0.3 mL) and 0.1 M KCl (2 mL). Another comparable test was a 4 mL aqueous solution of 0.01 M NaOH along with 3 mM of TA, 0.03 mM of H_2O_2 (0.3 mL), 0.1 M KCl (2 mL) and 2 mg of TiO_2@PMOS. Both samples were irradiated by visible light using a Tungsten bulb (200 W) with constant stirring in a 2 × 2 × 2.5 ft^3 dark box. After 20 min the photoluminescence spectra were recorded as shown in Fig. 5 and revealed.

Photocatalysis of organic pollutants by TiO_2@PMOS required energy to excite electrons from valence band (VB) to conduction band (CB) [29]. UV-irradiation full filled that energy demand and produced hydroxyl free radicals (•OH) after reacting at holes of VB with water molecules and hydroxyl ions. The dissolved oxygen molecules were also reduced by the electrons present in the CB of TiO_2@PMOS into $^{\bullet}O_2^-$ radicals that can also cause degradation [41]. However, most of $^{\bullet}O_2^-$ radicals were converted to highly reactive $^{\bullet}OH_2$ and then changed into H_2O_2 [42,43]. All the free radicals formed were short-lived due to unpaired electron, chiefly •OH radicals were highly reactive and degraded the MO as expected in Fig. 5. The formation of the excessive hydroxyl free radicals (•OH) by TiO_2@PMOS and H_2O_2 was also monitored and shown in Fig. 5 by producing an intense fluorescent material hydroxyterephthalic acid (TAOH) from terephthalic acid (TA).

3.4. Photocatalytic activity of TiO_2@PMOS

Degradation of methyl orange was used to investigate the photocatalytic activity of TiO_2@PMOS under visible and UV-irradiation.

The demonstrative experiment was performed to examine the photolytic efficiency of TiO_2@PMOS. In a typical procedure, 30 mL of 20 ppm solution of MO was used to check degradation ability by using 12 mg of TiO_2@PMOS at a pH of 2. The whole assembly was kept in the dark box of 2 × 2 × 2.5 ft^3 dimensions fitted with UV-visible light sources for 1 h with continuous stirring in order to get absorption data after attaining adsorption–desorption equilibrium.

The samples were irradiated by a Tungsten bulb of 200 W and UV-A lamp as UV-visible light sources for 1 h to record the absorption values. Moreover, the samples were again irradiated with visible and UV-lights for 1 h

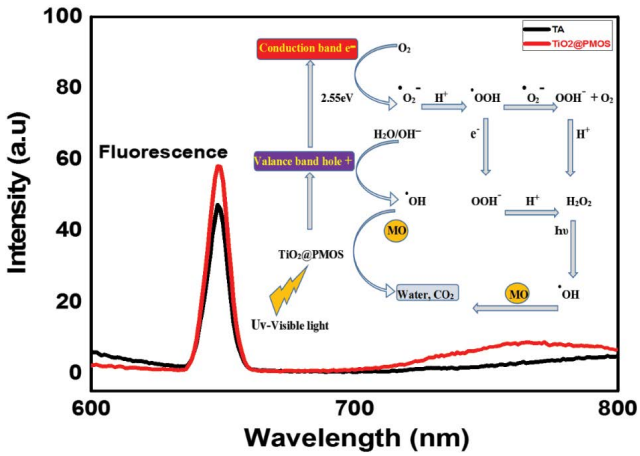

Fig. 5. PL results of terephthalic acid (TA) solution with and without TiO_2@PMOS and degradation mechanism.

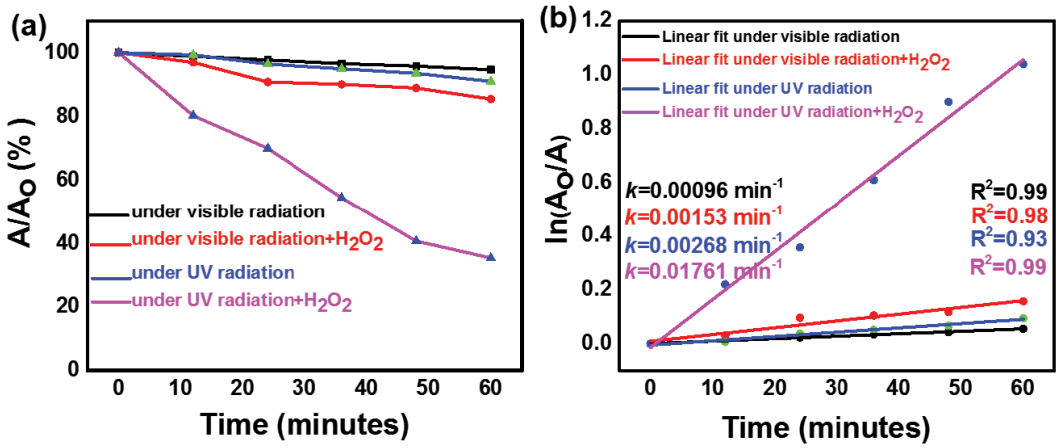

Fig. 6. (a) Photo-degradation competencies and (b) linear fit results of TiO_2@PMOS without and with H_2O_2 under visible and UV-irradiations.

after the addition of 0.3 mL H_2O_2 (0.03 M). The UV-visible spectrophotometer was used to scan all the samples which showed characteristic absorptions near-visible regions (Figs. S5 and S6). The absorption data was collected with time intervals of 0, 12, 24, 36, 48 and 60 min respectively.

The photocatalytic efficiency of TiO_2@PMOS was also assessed in terms of rate constant (k) of pseudo-first-order reaction. After subtracting dark adsorptions, the values of rate constants were 0.00096 and 0.00153 min^{-1} under visible- and UV-light respectively (Fig. 6b). However, the rate constant values were increased to 2.79 and 11.5 times after adding H_2O_2 which were 0.00268 and 0.01761 min^{-1} (Fig. 6b) under visible and UV-conditions respectively. The improved strengths of reaction rates by using H_2O_2 showed a large formation of active intermediates in which hydroxyl free radicals were dominant. The overall performance of TiO_2@PMOS under UV-light to remove MO in the absence and presence of H_2O_2 was 9.02% and 64.63% respectively. Likewise, the degradation efficiencies of TiO_2@PMOS under UV-light without and with H_2O_2 were 0.15 and 1.07 mg of MO per mg of TiO_2@PMOS respectively. These results were in good agreement with the effective degradation of TiO_2@PMOS compared to some previously reported material shown in Table 1 that made these materials more effective and durable to reuse in catalytic studies.

3.5. Reusability of catalyst

TiO_2@PMOS was recollected by centrifuging all the used samples, successively washed with distilled water and dried to reuse it. The catalytic experiment was repeated several times under optimized conditions [29] to observe photolytic activity of the regenerated TiO_2@PMOS. The UV-visible spectrophotometer showed the characteristic absorption even after fifth recycle (Fig. S8a). The absorption data collected after time intervals of 00 and 60 min was found to be 51% degradation of MO (Fig. 7). The results showed that the efficiency of TiO_2@PMOS was decreased only 20% after five consecutive cycles. The comparative degradation competency of TiO_2@PMOS reused made it more effective to recycle several times in catalytic studies.

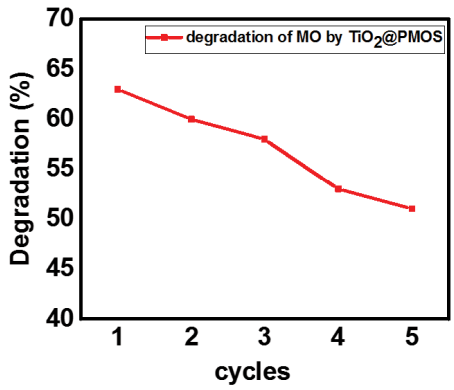

Fig. 7. Photo-degradation of MO by recycled TiO_2@PMOS.

4. Conclusions

The sol–gel technique was found to be much effective to produce periodic mesoporous organosilicates.

Table 1
Reaction kinetics comparison of photocatalytic degradation

Catalyst (conc.)	Removal (%)	Time (h)	k_{app} (min^{-1})	Reference
PAM-TiO_2 NC and porous TiO_2 beads	16.2% and 32.8%	01	0.00016 and 0.00248	[29]
TiO_2@PMOS (PMOS: Polyacrylamide) Nanocomposite	14.55% and 63.64%	01	0.00153 and 0.0176	Present work

A similar kind of practice was done in the present study by co-condensation of low-cost sodium silicate as silicon-precursor using polysorbate 80 templates. The colloidal solution of PMOS was used to soak TiO_2 in and onto the PMOS-surfaces to prepare TiO_2 subsidized PMOS and their characteristics result demonstrated the successful incorporation of organic and metal moieties in and onto the channels of synthesized materials. Subsequently, the TiO_2@PMOS exposed a higher potential to lessen MO with H_2O_2 under visible and UV light irradiation due to the large production of hydroxyl radicals as discussed earlier. These results indicated high surface area, reasonable bandgap and systematized nature of TiO_2@PMOS. Furthermore, the impressive degradation by reuse TiO_2@PMOS indicated their long-time durability. The effective outcomes open new platforms for impressive photo-degradation that made the current work innovative to synthesize the harmless and cost-effective metal-based periodic mesoporous organosilica for photo-degradation of organic azo dyes as well as other organic pollutants.

Acknowledgments

The authors are highly thankful to Higher Education Commission (HEC) of Pakistan and Islamia University of Bahawalpur (IUB), Pakistan for financial support.

References

[1] P. Hankare, A. Jadhav, R. Patil, K. Garadkar, I. Mulla, R. Sasikala, Photocatalytic degradation of rose bengal in visible light with Cr substituted $MnFe_2O_4$ ferrospinel, Arch. Phys. Res., 3 (2012) 269–276.
[2] U.G. Akpan, B.H. Hameed, Parameters affecting the photocatalytic degradation of dyes using TiO_2-based photocatalysts: a review, J. Hazard. Mater., 170 (2009) 520–529.
[3] M.A. Ahmad, R. Alrozi, Removal of malachite green dye from aqueous solution using rambutan peel-based activated carbon: equilibrium, kinetic and thermodynamic studies, Chem. Eng. J., 171 (2011) 510–516.
[4] A. Habibi-Yangjeh, S. Asadzadeh-Khaneghah, S. Feizpoor, A. Rouhi, Review on heterogeneous photocatalytic disinfection of waterborne, airborne, and foodborne viruses: can we win against pathogenic viruses?, J. Colloid Interface Sci., 580 (2020) 503–514.
[5] M. Kulkarni, P. Thakur, Photocatalytic degradation and mineralization of reactive textile azo dye using semiconductor metal oxide nano particles, Int. J. Eng. Res. Gen. Sci., 2 (2014) 245–254.
[6] M. Shekofteh-Gohari, A. Habibi-Yangjeh, M. Abitorabi, A. Rouhi, Magnetically separable nanocomposites based on ZnO and their applications in photocatalytic processes: a review, Crit. Rev. Env. Sci. Technol., 48 (2018) 806–857.
[7] M. Pirhashemi, A. Habibi-Yangjeh, S.R. Pouran, Review on the criteria anticipated for the fabrication of highly efficient ZnO-based visible-light-driven photocatalysts, J. Ind. Eng. Chem., 62 (2018) 1–25.
[8] S. Inagaki, S. Guan, Y. Fukushima, T. Ohsuna, O. Terasaki, Novel mesoporous materials with a uniform distribution of organic groups and inorganic oxide in their frameworks, J. Am. Chem. Soc., 121 (1999) 9611–9614.
[9] B.Y. Guan, Y. Cui, Z.Y. Ren, Z.-a. Qiao, L. Wang, Y.L. Liu, Q.S. Huo, Highly ordered periodic mesoporous organosilica nanoparticles with controllable pore structures, Nanoscale, 4 (2012) 6588–6596.
[10] S. Asadzadeh-Khaneghah, A. Habibi-Yangjeh, g-C_3N_4/carbon dot-based nanocomposites serve as efficacious photocatalysts for environmental purification and energy generation: a review, J. Cleaner Prod., 276 (2020) 124319, doi: 10.1016/j.jclepro.2020.124319.
[11] A. Akhundi, A. Habibi-Yangjeh, M. Abitorabi, S. Rahim Pouran, Review on photocatalytic conversion of carbon dioxide to value-added compounds and renewable fuels by graphitic carbon nitride-based photocatalysts, Catal. Rev., 61 (2019) 595–628.
[12] A. Akhundi, A. Badiei, G.M. Ziarani, A. Habibi-Yangjeh, M.J. Muñoz-Batista, R. Luque, Graphitic carbon nitride-based photocatalysts: toward efficient organic transformation for value-added chemicals production, Mol. Catal., 488 (2020) 110902, doi: 10.1016/j.mcat.2020.110902.
[13] J.S. Beck, J.C. Vartuli, W.J. Roth, M.E. Leonowicz, C.T. Kresge, K.D. Schmitt, C.T.W. Chu, D.H. Olson, E.W. Sheppard, S.B. McCullen, J.B. Higgins, J.L. Schlenker, A new family of mesoporous molecular sieves prepared with liquid crystal templates, J. Am. Chem. Soc., 114 (1992) 10834–10843.
[14] Y.-y. Zhou, X.-x. Li, Z.-x. Chen, Rapid synthesis of well-ordered mesoporous silica from sodium silicate, Powder Technol., 226 (2012) 239–245.
[15] N. Mizoshita, T. Tani, S. Inagaki, Syntheses, properties and applications of periodic mesoporous organosilicas prepared from bridged organosilane precursors, Chem. Soc. Rev., 40 (2011) 789–800.
[16] M. Rat, M.H. Zahedi-Niaki, S. Kaliaguine, T.-O. Do, Sulfonic acid functionalized periodic mesoporous organosilicas as acetalization catalysts, Microporous Mesoporous Mater., 112 (2008) 26–31.
[17] C.M. Li, J. Liu, L. Zhang, J. Yang, Q.H. Yang, Mesoporous organosilicas containing disulfide moiety: synthesis and generation of sulfonic acid functionality through chemical transformation in the pore wall, Microporous Mesoporous Mater., 113 (2008) 333–342.
[18] B. Karimi, M. Gholinejad, M. Khorasani, Highly efficient three-component coupling reaction catalyzed by gold nanoparticles supported on periodic mesoporous organosilica with ionic liquid framework, Chem. Commun., 48 (2012) 8961–8963.
[19] A. Modak, M. Nandi, A. Bhaumik, Titanium containing periodic mesoporous organosilica as an efficient catalyst for the epoxidation of alkenes, Catal. Today, 198 (2012) 45–51.
[20] S. Nasreen, U. Rafique, S. Ehrman, M.A. Ashraf, Hybrid mesoporous silicates: a distinct aspect to synthesis and application for decontamination of phenols, Saudi J. Biol. Sci., 26 (2019) 1161–1170.
[21] V. Lygin, The structure of the silica surface and its modification by thermal treatment, Kinet. Catal., 35 (1994) 480–486.
[22] L.N.H. Arakaki, L.M. Nunes, J.A. Simoni, C. Airoldi, Ethyleneimine anchored on thiol-modified silica gel surface—adsorption of divalent cations and calorimetric data, J. Colloid Interface Sci., 228 (2000) 46–51.
[23] B. Buszewski, M. Jezierska, M. Wełniak, D. Berek, Survey and trends in the preparation of chemically bonded silica phases for liquid chromatographic analysis, J. High. Resolut. Chromatogr., 21 (1998) 267–281.
[24] E.-B. Cho, D.J. Kim, M. Jaroniec, Monodisperse particles of bifunctional periodic mesoporous organosilica, J. Phys. Chem. C, 112 (2008) 4897–4902.
[25] T. Asefa, M.J. MacLachlan, N. Coombs, G.A. Ozin, Periodic mesoporous organosilicas with organic groups inside the channel walls, Nature, 402 (1999) 867–871.
[26] B. Karimi, F.K. Esfahani, Unexpected golden Ullmann reaction catalyzed by Au nanoparticles supported on periodic mesoporous organosilica (PMO), Chem. Commun., 47 (2011) 10452–10454.
[27] K. Sinkó, Influence of chemical conditions on the nanoporous structure of silicate aerogels, Materials, 3 (2010) 704–740.
[28] F. Rajabi, A.Z. Ebrahimi, A. Rabiee, A. Pineda, R. Luque, Synthesis and characterization of novel pyridine periodic mesoporous organosilicas and its catalytic activity in the knoevenagel condensation reaction, Materials, 13 (2020) 1097, doi: 10.3390/ma13051097.
[29] M.A. Mudassir, S.Z. Hussain, M. Khan, S.T. Asma, Z. Iqbal, Z. Huma, N. Ullah, H. Zhang, T.M. Ansari, I. Hussain,

Polyacrylamide exotemplate-assisted synthesis of hierarchically porous nanostructured TiO_2 macrobeads for efficient photodegradation of organic dyes and microbes, RSC Adv., 8 (2018) 29628–29636.
[30] K. Narasimharao, T.T. Ali, S. Bawaked, S. Basahel, Effect of Si precursor on structural and catalytic properties of nanosize magnesium silicates, Appl. Catal., A, 488 (2014) 208–218.
[31] B.W. Lee, Y.H. Kim, H.J. Lee, J. Yi, Synthesis of functionalized porous silicas via templating method as heavy metal ion adsorbents: the introduction of surface hydrophilicity onto the surface of adsorbents, Microporous Mesoporous Mater., 50 (2001) 77–90.
[32] A.S. Piers, C.H. Rochester, Infrared study of the adsorption of 1-aminopropyltrialkoxysilanes on silica at the solid/liquid interface, J. Colloid Interface Sci., 174 (1995) 97–103.
[33] Y. Mori, T.J. Pinnavaia, Optimizing organic functionality in mesostructured silica: direct assembly of mercaptopropyl groups in wormhole framework structures, Chem. Mater., 13 (2001) 2173–2178.
[34] H.H.P. Yiu, C.H. Botting, N.P. Botting, P.A. Wright, Size selective protein adsorption on thiol-functionalised SBA-15 mesoporous molecular sieve, Phys. Chem. Chem. Phys., 3 (2001) 2983–2985.
[35] T.-S. Deng, Q.-F. Zhang, J.-Y. Zhang, X. Shen, K.-T. Zhu, J.-L. Wu, One-step synthesis of highly monodisperse hybrid silica spheres in aqueous solution, J. Colloid Interface Sci., 329 (2009) 292–299.
[36] L. dos Santos Andrade, B. Castanheira, S. Brochsztain, Periodic mesoporous organosilicas containing naphthalenediimides within the pore walls for asphaltene adsorption, Microporous Mesoporous Mater., 294 (2020) 109909, doi: 10.1016/j.micromeso.2019.109909.
[37] T. Qureshi, N. Memon, S.Q. Memon, M.A. Ashraf, Decontamination of ofloxacin: optimization of removal process onto sawdust using response surface methodology, Desal. Water Treat., 57 (2016) 221–229.
[38] K.V. Bineesh, D.-K. Kim, D.-W. Park, Synthesis and characterization of zirconium-doped mesoporous nano-crystalline TiO_2, Nanoscale, 2 (2010) 1222–1228.
[39] L. Zhang, S.Z. Qiao, Y.G. Jin, Z.G. Chen, H.C. Gu, G.Q. Lu, Magnetic hollow spheres of periodic mesoporous organosilica and Fe_3O_4 nanocrystals: fabrication and structure control, Adv. Mater., 20 (2008) 805–809.
[40] Y.-Y. Song, P. Roy, I. Paramasivam, P. Schmuki, Voltage-induced payload release and wettability control on TiO_2 and TiO_2 nanotubes, Angew. Chem. Int. Ed., 49 (2010) 351–354.
[41] W.B. Dong, D.B. Wang, H. Wang, M.K. Li, F. Chen, F.Y. Jia, Q. Yang, X.M. Li, X.Z. Yuan, J. Gong, H.L. Li, J. Ye, Facile synthesis of In_2S_3/UiO-66 composite with enhanced adsorption performance and photocatalytic activity for the removal of tetracycline under visible light irradiation, J. Colloid Interface Sci., 535 (2019) 444–457.
[42] W.A. Daoud, J.H. Xin, Y.-H. Zhang, Surface functionalization of cellulose fibers with titanium dioxide nanoparticles and their combined bactericidal activities, Surf. Sci., 599 (2005) 69–75.
[43] O. Seven, B. Dindar, S. Aydemir, D. Metin, M.A. Ozinel, S. Icli, Solar photocatalytic disinfection of a group of bacteria and fungi aqueous suspensions with TiO_2, ZnO and Sahara desert dust, J. Photochem. Photobiol., A, 165 (2004) 103–107.
[44] W.J. Tan, J.R. Peralta-Videa, J.L. Gardea-Torresdey, Interaction of titanium dioxide nanoparticles with soil components and plants: current knowledge and future research needs–a critical review, Environ. Sci. Nano, 5 (2018) 257–278.
[45] S. Yaparatne, C.P. Tripp, A. Amirbahman, Photodegradation of taste and odor compounds in water in the presence of immobilized TiO_2-SiO_2 photocatalysts, J. Hazard. Mater., 346 (2018) 208–217.

Supporting information

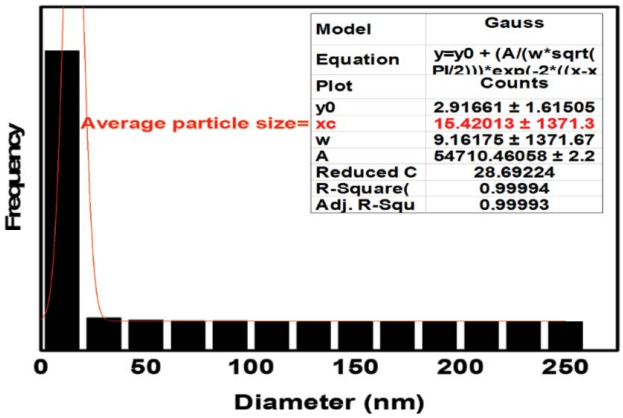

Fig. S1. The average particle size of PMOS calculated by ImageJ software using TEM images.

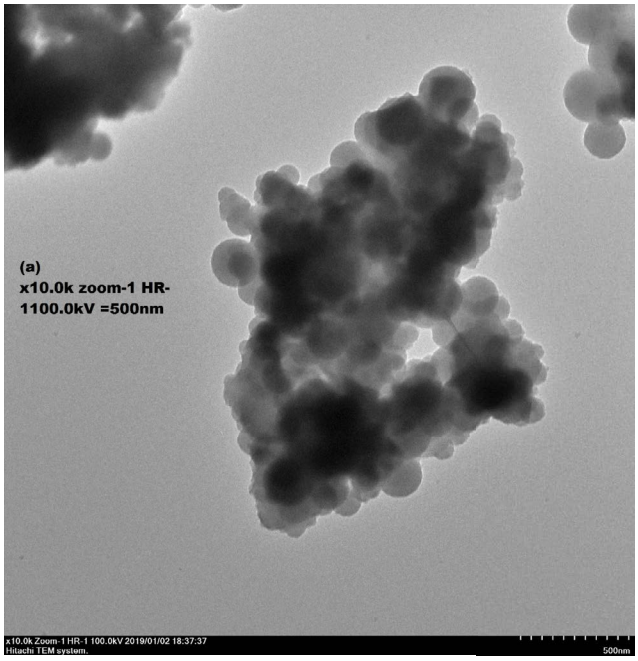

Fig. S2. TEM image of PMOS with 10.0 zoom.

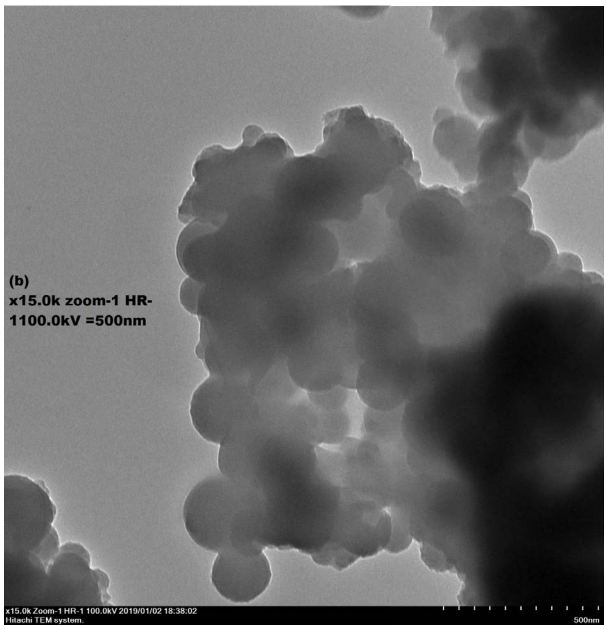

Fig. S3. TEM image of PMOS with 15.0 zoom.

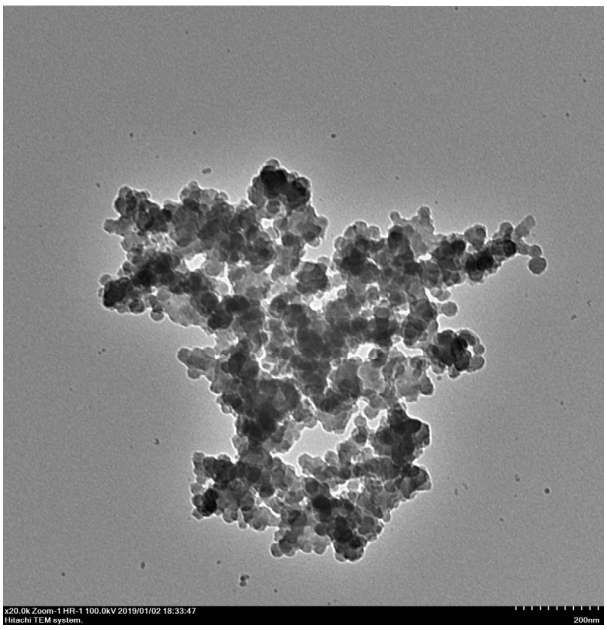

Fig. S4. TEM image of TiO_2@PMOS.

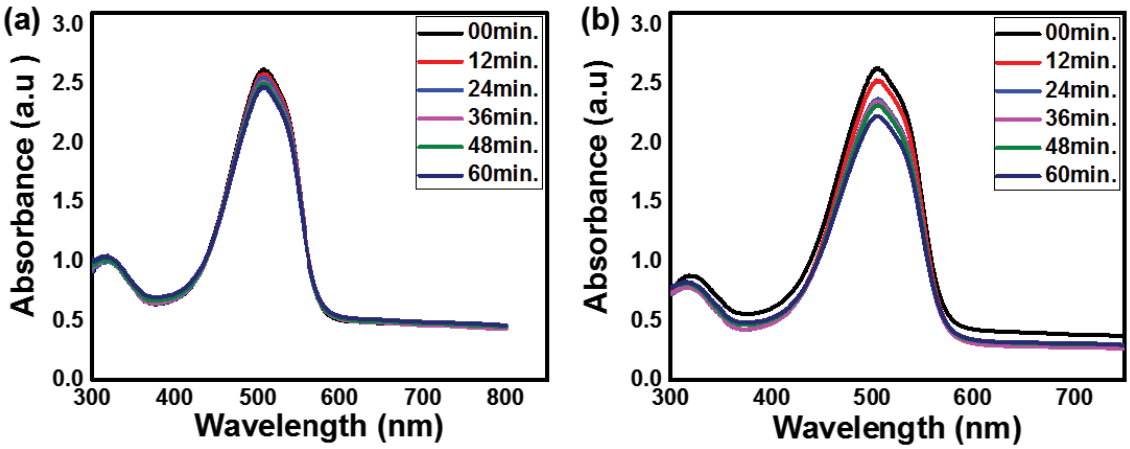

Fig. S5. UV-visible spectra for photocatalysis of TiO_2@PMOS without (a) H_2O_2 and with (b) H_2O_2 under visible irradiation.

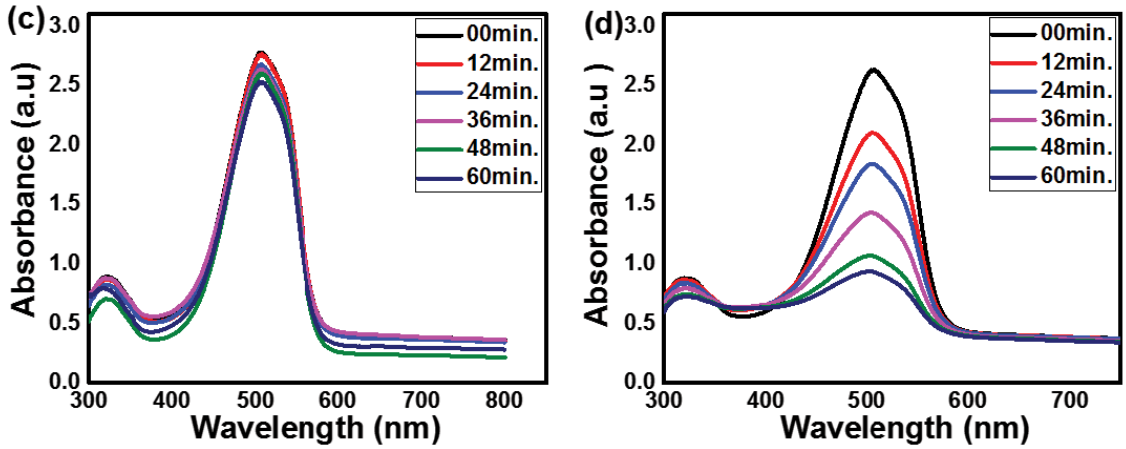

Fig. S6. UV-visible spectra for photocatalysis of TiO_2@PMOS without (c) H_2O_2 and with (d) H_2O_2 under UV-irradiation.

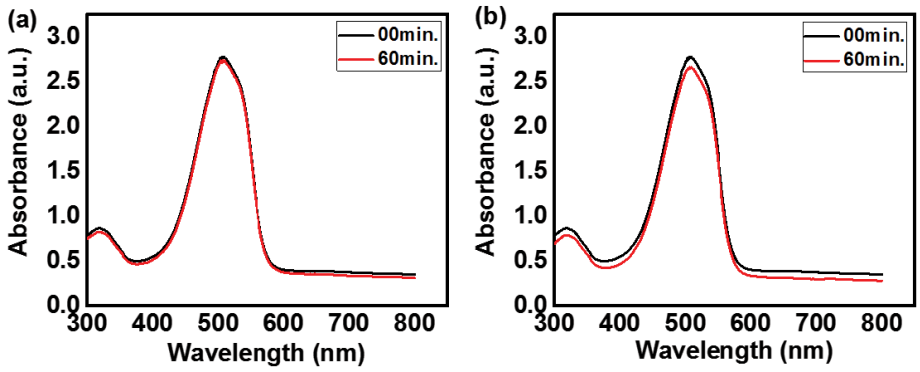

Fig. S7. UV-visible spectra for photocatalysis of blanks (a) TiO_2 and (b) H_2O_2.

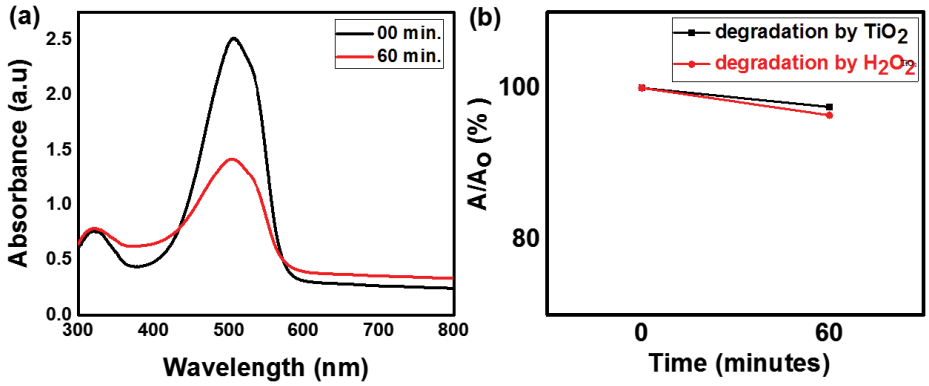

Fig. S8. (a) UV-visible spectra of the 5th cycle by TiO_2@PMOS and (b) percentage degradation of blanks (TiO_2 and H_2O_2).

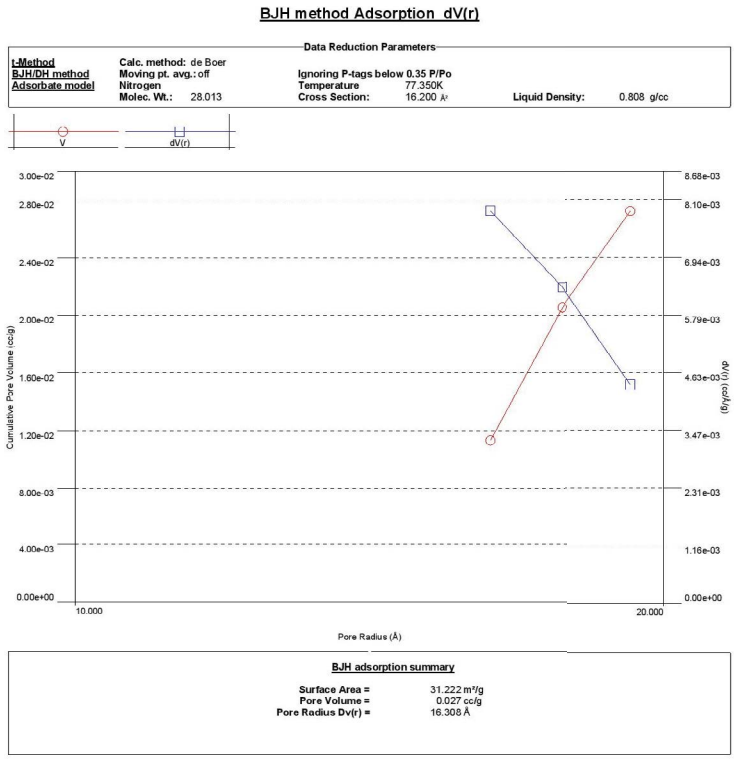

Fig. S9. Barrett–Joyner–Halenda graphs PMOS.

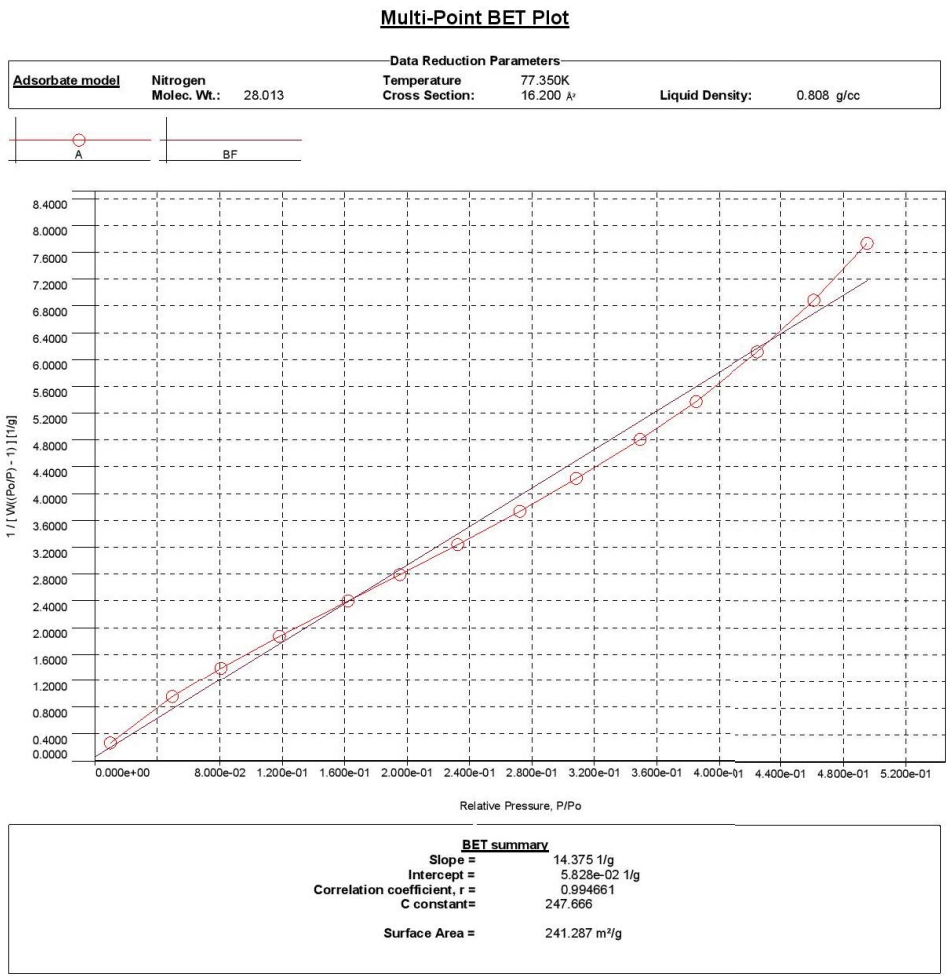

Fig. S10. BET graphs showing the surface area of PMOS.